Nanoscale Imaging and Spectroscopy of Plasmonic Modes with the PTIR Technique

*Aaron M. Katzenmeyer, Jungseok Chae, Richard Kasica, Glenn Holland, Basudev Lahiri, and Andrea Centrone**

The collective oscillation of conduction electrons in plasmonic nanomaterials allows the coupling of propagating light waves with nanoscale volumes of matter ("hot spots") and allows engineering the optical response of these materials from the UV to THz as a function of nanostructure size and shape. These properties can be leveraged for important applications such as sensing,[1] photovoltaics,[2] cloaking[3] and therapeutics.[4] For example, plasmonic nanostructures with resonances in the mid-infrared enable surface-enhanced infrared absorption (SEIRA),[1b,5] increasing the chemical detection limits of IR spectroscopy up to the zeptomolar range.[1a] Despite numerous practical applications only a few experimental techniques are available to characterize plasmonic materials with high spatial resolution.[1b,6] For example, scattering type scanning near-field optical microscopy (s-SNOM) measures the light scattered by an atomic force microscope (AMF) tip in proximity of a sample and has been successfully used to map the near-field properties of plasmonic structures. However, the limited wavelength tunability of s-SNOM IR sources allowed for the interrogation of plasmonic structures at only one[7] or a few wavelengths[6b] or as a convolution of broad-band excitation.[8] In any case, the spectrum of a plasmonic structure in the near-field has not been reported yet and theoretical calculations are typically necessary to guide experiments, extract meaningful data,[9] and put the sparse experimental points into context. On the contrary, by measuring the near-field absorption[10] (not scattering), the photothermal induced resonance (PTIR)[1b,10,11] technique allows nanoscale resolution imaging and spectroscopy over the whole mid-IR spectral range.[12] In this work, we apply the PTIR technique to obtain the first near-field absorption spectra of gold asymmetric split ring resonators (ASRRs)[13] and to image their plasmonic modes. Since the PTIR spectra are not affected by scattered field,[1b] the absorption properties of plasmonic nanostructures can be obtained without the spectral profile complexities of Fano resonances typically observed in s-SNOM and far-field spectroscopies. With this contribution, we show that in addition to insulators[12] and semiconductors,[14] metals are also amenable to PTIR characterization, an important step forward to apply the PTIR technique to a wide variety of functional devices.

PTIR[1b,10,11] combines the lateral resolution of atomic force microscopy (AFM) with the chemical specificity of IR absorption spectroscopy, breaking the diffraction limit of IR light and enabling materials identification at the nanoscale by direct comparison with IR spectral libraries.[15] PTIR uses a tunable pulsed laser for sample illumination and an AFM tip in contact mode as a mechanical detector for extracting local spectral information. PTIR samples are placed or fabricated on an optically transparent prism and are illuminated by total internal reflection to minimize the direct light-tip interaction (**Figure 1**a). The absorption of a laser pulse by the sample under the tip causes local heating, sample expansion, and the mechanical excitation of the AFM cantilever. A four-quadrant detector monitors the cantilever deflection as a function of time by measuring the position of the AFM laser reflecting from the cantilever. The local infrared absorption spectrum is obtained by determining the maximum amplitude of the tip deflection (Figure 1b) as a function of wavelength. PTIR images are obtained by illuminating the sample at a fixed wavelength while scanning the AFM tip.[10,12,16] Because of the low laser repetition rate (1 kHz), each new pulse excites the sample and cantilever only after they have returned to equilibrium. A zinc selenide lens is used to focus the light under the AFM tip while a polarization control module consisting of a set of three mirrors controls the polarization of linearly polarized light at the sample. The typical laser spot size is ≈30 μm, but the AFM tip functions as a "spatial filter" allowing the extraction of spectroscopic information with nanoscale resolution, much smaller than the diffraction limit of IR light.[10,11b,15] PTIR has been applied for nanoscale characterization of bacteria,[11b,16] polymers,[10,12,15,17] metal-organic frameworks,[18] inorganic particles,[12,14] and cells.[19] Using tunable laser sources with a repetition rate that matches one of the AFM cantilever mechanical resonance self-assembled monolayers could also be measured.[20] Very recently, the PTIR technique was applied to characterize gold asymmetric split ring resonators arrays[1b] and quantify the SEIRA enhancement in the near-field for the first time. We named this technique Surface Enhanced PTIR (SE-PTIR).[1b] However, the PTIR signal intensity, proportional to the linear expansion coefficient (α) and inversely proportional to the thermal conductivity (η) of the sample,[12,21] makes the direct measurement of metallic structures (small α and large η) challenging. Previously, to overcome these limitations, the large α of polymer films was exploited to mechanically amplify the PTIR signal of underlying

Dr. A. M. Katzenmeyer, Dr. J. Chae, R. Kasica, G. Holland, Dr. B. Lahiri, Dr. A. Centrone
Center for Nanoscale Science and Technology
National Institute Standards and Technology
Gaithersburg, 100 Bureau Drive, Maryland 20899, USA
E-mail: andrea.centrone@nist.gov
Dr. J. Chae, Dr. B. Lahiri
Maryland Nanocenter
University of Maryland
College Park, MD 20742, USA

DOI: 10.1002/adom.201400005

© 2014 WILEY-VCH Verlag GmbH & Co. KGaA, Weinheim

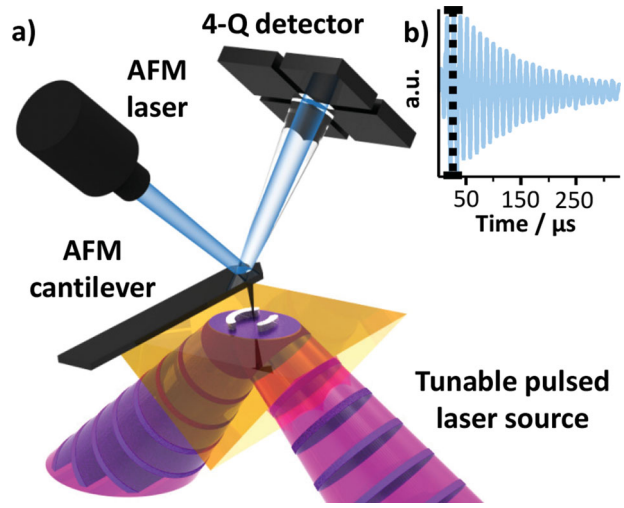

Figure 1. a) Schematic of the PTIR measure: The pulsed IR laser beam (purple discs within the pink envelope) illuminates the sample via total internal reflection. The absorption of a laser pulse in the sample causes the sample to thermally expand and deflects the AFM cantilever proportionally to the absorbed energy. The cantilever deflection is measured with a four-quadrant detector that monitors the position of the AFM laser reflecting from the AFM cantilever. b) PTIR deflection signal as a function time. The maximum amplitude of the tip deflection was used to obtain PTIR maps and spectra.

metallic structures and indirectly image their plasmonic modes.[1b] However, for such a system, the very large SE-PTIR signal due to direct absorption in the polymer layer overwhelms the indirectly measured plasmon absorption when the two spectrally overlap, thus preventing the acquisition of near-field plasmonic spectra and limiting the ability of imaging the plasmonic modes to spectral regions where the polymer absorption is negligible.[1b] The results presented here show that PTIR can indeed be used to directly interrogate metallic structures, offering improved spatial resolution to map the near-field absorption in these materials. Additionally, PTIR spectra of the plasmonic structures can now be collected directly without the limitations imposed by the spectral overlap with the polymer film. Such investigation was possible due to improved procedures for both alignment of the IR laser and signal optimization (see the Supporting Information experimental information for details).

ASRRs[13] are plasmonic structures composed of two metallic arcs with a common center. By changing the resonator diameter it is possible to tune the resonator's plasmonic resonances across the whole mid-IR spectral range[1b] a characteristic that can be exploited for increasing the sensitivity of IR spectroscopy via the SEIRA effect.[1b,5] To allow PTIR measurements, the gold resonators arrays were fabricated directly on zinc selenide right angle prisms with a combination of electron beam lithography and lift-off (see supplemental information),[1b] using custom adaptor pieces described previously.[10] In this work we study the absorption properties in the near-field of an asymmetric split ring resonators array (hereafter ASRR-1) characterized by resonators with an external diameter of 1900 nm ± 45 nm, a thickness of 100 nm ± 10 nm, and a pitch of or 12 µm ± 0.06 µm as determined by AFM. Another three samples were prepared and characterized in the far-field, namely: an array consisting of the ASRR's left arc only, an array consisting of the ASRR's right arc only, and an ASRRs array (ASRR-ref) used for reference, made by arcs with the same size of the left arc only and right arc only samples. The pitch in these three arrays was 10 µm ± 0.07 µm. The ASRR-ref sample has external diameter of 1790 nm ± 11 nm and a thickness of 120 nm ± 5 nm. On both ASRR-1 and ASRR-ref, protrusions up to about 50 nm are common at the edges due to non-perfect lift off during fabrication. The uncertainties in the resonator diameter, pitch, and height correspond to a single standard deviation as measured by AFM and arise mostly from the nanofabrication process. The plasmonic response of the resonators is strongly polarization dependent and for linear polarization it is stronger for polarization parallel to the long direction of the arcs, hereafter parallel polarization. All FTIR and PTIR experiments were recorded using light with parallel polarization.

It is well known that the plasmonic modes of metallic structures in close proximity couple via near-field interactions and that their resulting optical properties are well described by the plasmon hybridization model.[22] According to this model the plasmonic resonances of each individual arc in an A-SRR hybridize leading to a lower energy antisymmetric and a higher energy symmetric collective modes.[1b,22a] The constructive and destructive interference of the broader symmetric "bright" mode with the narrower anti-symmetric "dark" mode[2,23] generates two maxima and a minimum in the resonators' far-field reflection spectra (**Figure 2**). In particular, such interference leads to a Fano-shaped profile which makes plasmonic peaks sharper and increases their *Q*-factor with respect to their symmetric counterparts due to low scattering losses of the dark-mode.[23] The interference between the bright and dark mode that generates the Fano distortion, makes the far-field spectral response of the resonators different than the bare sum of the response originating from the individual arcs' (Figure 2).

In contrast with the far-field reflection spectra, no Fano distortion is observed in the PTIR spectra (see **Figure 3**a) because the PTIR signal is proportional to the product of the optical power density and plasmon absorption coefficient[1b] while it is independent of scattering. Furthermore, the PTIR technique not only improves the spatial resolution of IR spectroscopy but also greatly improves its sensitivity, even for samples with relatively unfavorable thermo-mechanical properties like gold. For example, the far-field FTIR reflectance spectra of the ASRR-1 array, obtained by averaging the response of approximately 200 resonators (see Figure S1) requires averaging hundreds of spectra to achieve a signal to noise ratio comparable to that obtained by averaging four PTIR spectra which measure the response of a single resonator in the same array (Figure 3a). Importantly, while probed locally, the PTIR spectrum is characteristic of the resonator's collective plasmonic modes, not of the constituent isolated arc. For example, the spectral intensity of the resonator's PTIR spectrum is much larger than that of individual arcs, which were not measurable under the experimental condition used in this work, because of the large absorption coefficient due to the resonators' dark-mode.

Finite-element-method calculations suggested[1b] that under the conditions of PTIR experiments (45° angle illumination) the energy absorbed by the arcs is mostly due to the dark-mode

© 2014 WILEY-VCH Verlag GmbH & Co. KGaA, Weinheim

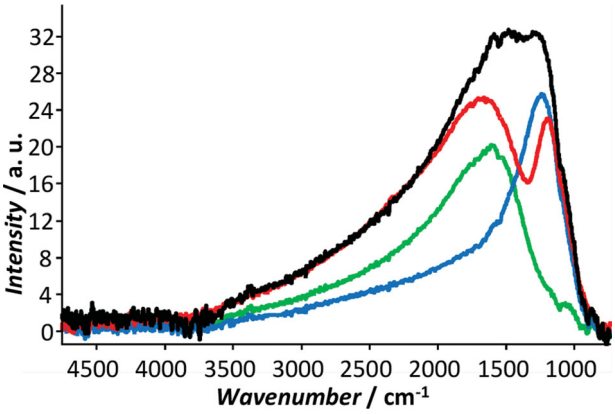

Figure 2. Far-field FTIR reflection spectra for: ASRR-ref array (red), left arcs only array (LA, blue), right arcs only array (RA, green), and calculated intensity sum of the individual arcs (LA+RA) arrays (black).

excitation. However, because of their spectral overlap, the bright and dark modes interfere. At longer wavelengths the dark-mode is excited almost exclusively and a larger fraction of the optical power is dissipated by the longer arc. At shorter wavelengths, the interference of the dark-mode with a small admixture of the bright-mode increases the power dissipated by the short arc and suppresses the power dissipated by the long one. In between, the energy dissipated in each arc changes as a result of the interference of the two modes. The PTIR images (Figure 3b–f) display the energy dissipated within the arcs due to the plasmonic excitation[24] providing evidence of the interference between the two modes. The PTIR spectra (Figure 3a) identify the cross over between the energy density dissipated in the two arcs at 7.2 μm (1384 cm^{-1}). Based on this local spectroscopic information a shift from dissipation predominantly in the shorter right arc at shorter wavelengths to dissipation predominantly in the longer left arc for longer wavelengths is expected. Such behavior is clearly supported by the PTIR maps in Figure 3b–f (displayed in full scale). For example, at shorter wavelengths (1472 cm^{-1}, Figure 3b and 1432 cm^{-1}, Figure 3c), the dissipation is primarily localized in the shorter right arc. As expected, at 1384 cm^{-1} (Figure 3d) both arcs are equally excited. At longer wavelengths, (1268 cm^{-1}, Figure 3e and 1184 cm^{-1}, Figure 3f) the dissipation occurs predominantly in the longer left arc. The same maps are plotted in common intensity scale after normalization with respect to incident laser power in the supplemental information (Figure S2). Such images show that the stronger absorption occurs at ≈1268 cm^{-1} and that it is localized predominantly in the longer left arc which is consistent with the PTIR spectra (Figure 3a). Such spectra represent an important step forward in IR plasmonic research as they not only confirm the prediction of previous finite-element calculations[1b] but also offer standalone experimental guidance for imaging plasmonic modes in the near-field.

Overcoming the need of a polymeric mechanical amplification layer and measuring the resonators directly allows resolving the mode structure of the plasmonic excitation better which could be beneficial to understand the role of fabrication defects in the resonator's response. For example, PTIR maps in reference[1b] revealed subtle differences in the response of one ASRR with respect to another. We can now directly observe potential causes of such differences. See the left arc in Figure 3c and the right arc in Figure 3e in relation to the height image in Figure 3a (inset). The edge roughness resulting from the lift-off procedure contributes to local variation of signal intensity which may be expected to result in subtle differences in the resonators' response. Another benefit of mapping the plasmonic modes directly is the improved spatial resolution. For example, Figure 3f shows that the heating due to the plasmon excitation is strongest at the arc tips where the electric field is maximum. This type of excitation resembles the dipolar excitation observed in gold nanorods[7a] and may be speculatively attributed to a relatively localized thermal excitation. The comparison of height and PTIR line profiles (Figure S3) reveals that the PTIR mapping resolution is limited by the pixel size to ≈30 nm, an order of magnitude smaller than the arcs width. In contrast, the PTIR lateral resolution obtained when imaging the resonators' plasmonic modes coated by a polymer layer was limited by heat diffusion in the polymer layer to a value comparable with the polymer layer thickness (≈200 nm).[1b]

We believe that by measuring absorbed and scattered light respectively, PTIR and s-SNOM are complementary techniques for studying the near-field properties of materials. For example, the bright mode and the dark mode of plasmonic structures behave differently: the bright mode excitation results predominantly in scattered light and in little absorption while for the dark-mode the scattered light is much weaker and the absorbed light is strong.[1b] In contrast, the detection mechanism of

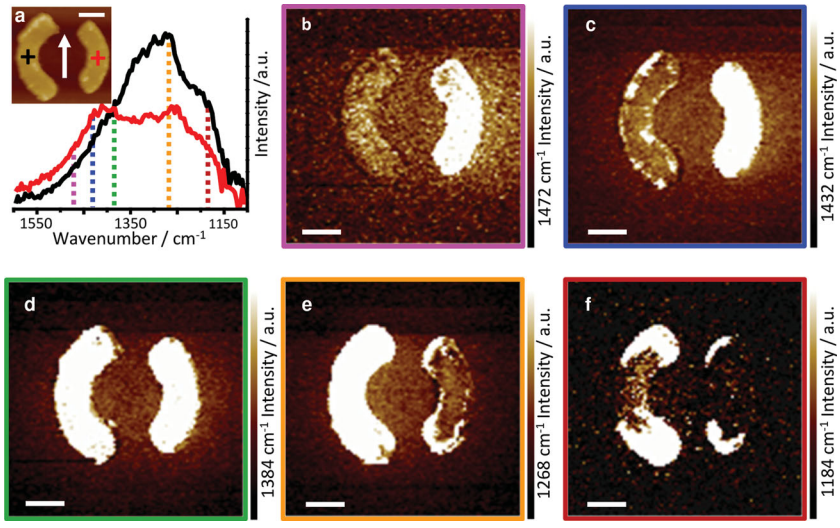

Figure 3. a) PTIR spectra of the ASRR-1 sample collected at locations identified by a color coded "+" in the inset height image. b–f) PTIR maps (each displayed with its own, unique full scale) emphasize the contribution of each arc to the collective modes of the resonator at several wavelengths of interest (identified by dotted color coded vertical lines in Figure 3a). All scale bars are 500 nm; the white arrow in the height inset indicates the direction of the electric field polarization in the PTIR experiments.

© 2014 WILEY-VCH Verlag GmbH & Co. KGaA, Weinheim

s-SNOM makes this technique typically more sensitive to the scattered light. More specifically, the scattered light detected in s-SNOM experiments is a complex function of tip-sample near-field interactions, the sample's local index of refraction, and the local absorption coefficient which necessitates non-trivial theoretical modelling to attempt the reconstruction of IR absorption spectra from the data. While such complexity if disentangled may provide a wealth of information about the sample's near-surface region, the simpler PTIR approach has several important characteristics which make its data immediately informative. Namely: (i) the topographic and the spectral information are acquired at different timescales preventing any crosstalk between the two channels,[1b] (ii) the PTIR spectra are a measure of sample absorption and can be used as is for materials identification via direct comparison with IR spectral databases,[15] (iii) the PTIR signal increases linearly with sample thickness up to ≈1 μm,[10] enabling nanoscale quantitative analysis. These characteristics, combined with the broad tunability of PTIR laser sources[12,25] make the PTIR technique a very useful tool for characterizing materials at the nanoscale.

In conclusion we applied the PTIR technique to directly characterize individual plasmonic nanostructures in the near-field with both high spectral and spatial resolution. This approach enabled the extraction of the first local near-field plasmonic IR absorption spectra, which are free of Fano-distortions. In particular, local PTIR spectra of A-SRRs predict well the crossover in the absorbed energy localization from short arc to long arc with increasing wavelength as a result of the interference between bright and dark modes. Such spectra provide guidance to map the energy dissipated in the resonators at wavelengths of interest without necessitating theoretical calculations. Here it is shown that in addition to insulators[12] and semiconductors[14] metals can also be measured with the PTIR technique, an important step forward in applying this characterization method to a variety of state-of-the-art functional devices (e.g. flexible electronics or nanocomposites) which synergistically combine diverse materials to engineer novel functionality.

Experimental Section

FTIR Spectroscopy: Fourier Transform Infrared (FTIR) spectra were recorded at near normal incidence with an FTIR spectrometer equipped with an infrared microscope by illuminating the entire array with a 36× reverse Cassegrain reflection objective (NA = 0.52) and a ZnSe wire grid polarizer (to control the light polarization). 512 spectra (4 cm^{-1} resolution) were acquired and averaged for each sample.

PTIR Experimental Set-up: PTIR experiments were carried out using a commercial PTIR setup which consists of an AFM microscope operating in contact mode and a tunable pulsed laser source consisting of an Optical Parametric Oscillator (OPO) based on a non-critically phase-matched $ZnGeP_2$ crystal. The laser emits pulses 10 ns long at 1 kHz repetition rate which are tunable from 4000 cm^{-1} to ≈1025 cm^{-1} (from 2.5 μm to 9.76 μm). The samples on a ZnSe prism were illuminated by total internal reflection (Figure 1a) focusing the laser light under the AFM tip with a ZnSe lens. The typical spot size is 30 μm ± 10 μm depending on the wavelength. The laser output is linearly polarized and a rotating ZnSe wire grid linear polarizer is used as a variable attenuator to control the light intensity. A polarization control module, consisting of three motorized mirrors, is used to obtain the desired polarization at the sample. Most of the optics in the PTIR setup and inside the laser are placed on motorized stages which allow automatic wavelength selection and sweeping via a computer interface. Since different wavelengths are typically emitted by the OPO at different angles, an infrared pyroelectric camera was used to calibrate the mirror positions resulting in the laser output co-linearity in the entire wavelength range.

PTIR Experiments: PTIR spectra were obtained by averaging the cantilever deflection amplitude from 256 individual laser pulses at each wavelength and tuning the laser at intervals of 4 cm^{-1}. Four consecutive spectra were averaged to increase the signal to noise ratio. PTIR images were recorded by illuminating the sample at constant wavelength while scanning the AFM tip in contact mode. The AFM height and the PTIR signal acquisition was synchronized so that for each AFM pixel the PTIR signal is an average over a fixed number of laser pulses[10] (64 in this work). The pixel sizes are 30 nm × 30 nm in all images. All PTIR experiments were recorded with linearly, s-polarized light with the electric field vector always in the resonators plane and parallel to the long direction of the arcs. Commercially available 450 μm long silicon contact-mode AFM probes with a nominal spring constant between 0.07 N/m and 0.4 N/m were used for this study.

Supporting Information

Supporting Information is available from the Wiley Online Library or from the author.

Acknowledgements

J. C. and B. L. acknowledge support under the Cooperative Research Agreement between the University of Maryland and the National Institute of Standards and Technology Center for Nanoscale Science and Technology, Award 70NANB10H193, through the University of Maryland.

Received: January 7, 2014
Revised: March 14, 2014
Published online: May 2, 2014

[1] a) R. Adato, A. A. Yanik, J. J. Amsden, D. L. Kaplan, F. G. Omenetto, M. K. Hong, S. Erramilli, H. Altug, *Proc. Natl. Acad. Sci. USA* **2009**, *106*, 19227; b) B. Lahiri, G. Holland, V. Aksyuk, A. Centrone, *Nano Lett.* **2013**, *13*, 3218; c) W. Bao M. Melli, N. Caselli, F. Riboli, D. S. Wiersma, M. Staffaroni, H. Choo, D. F. Ogletree, S. Aloni, J. Bokor, S. Cabrini, F. Intonti, M. B. Salmeron, E. Yablonovitch, P. J. Schuck, A. Weber-Bargioni, *Science* **2012**, *338*, 1317; d) J. N. Anker, W. P. Hall, O. Lyandres, N. C. Shah, J. Zhao, R. P. Van Duyne, *Nat. Mater.* **2008**, *7*, 442; e) M. E. Stewart, C. R. Anderton, L. B. Thompson, J. Maria, S. K. Gray, J. A. Rogers, R. G. Nuzzo, *Chem. Rev.* **2008**, *108*, 494; f) G. von Maltzahn, A. Centrone, J. H. Park, R. Ramanathan, M. J. Sailor, T. A. Hatton, S. N. Bhatia, *Adv. Mater.* **2009**, *21*, 3175.

[2] H. A. Atwater, A. Polman, *Nat. Mater.* **2010**, *9*, 205.

[3] D. Schurig, J. Mock, B. Justice, S. Cummer, J. Pendry, A. Starr, D. Smith, *Science* **2006**, *314*, 977.

[4] a) L. R. Hirsch, R. J. Stafford, J. A. Bankson, S. R. Sershen, B. Rivera, R. E. Price, J. D. Hazle, N. J. Halas, J. L. West, *Proc. Natl. Acad. Sci. USA* **2003**, *100*, 13549; b) J. H. Park, G. von Maltzahn, L. L. Ong, A. Centrone, T. A. Hatton, E. Ruoslahti, S. N. Bhatia, M. J. Sailor, *Adv. Mater.* **2010**, *22*, 880; c) G. von Maltzahn, J. H. Park, K. Y. Lin, N. Singh, C. Schwoppe, R. Mesters, W. E. Berdel, E. Ruoslahti, M. J. Sailor, S. N. Bhatia, *Nat. Mater.* **2011**, *10*, 545.

[5] a) K. Chen, R. Adato, H. Altug, *ACS Nano* **2012**, *6*, 7998; b) H. Aouani, H. Sipova, M. Rahmani, M. Navarro-Cia, K. Hegnerova, J. Homola, M. H. Hong, S. A. Maier, *ACS Nano* **2013**,

© 2014 WILEY-VCH Verlag GmbH & Co. KGaA, Weinheim

7, 669; c) C. H. Wu, A. B. Khanikaev, R. Adato, N. Arju, A. A. Yanik, H. Altug, G. Shvets, *Nat. Mater.* **2012**, *11*, 69.
[6] a) T. Zentgraf, J. Dorfmuller, C. Rockstuhl, C. Etrich, R. Vogelgesang, K. Kern, T. Pertsch, F. Lederer, H. Giessen, *Opt. Lett.* **2008**, *33*, 848; b) P. Alonso-Gonzalez, M. Schnell, P. Sarriugarte, H. Sobhani, C. Wu, N. Arju, A. Khanikaev, F. Golmar, P. Albella, L. Arzubiaga, F. Casanova, L. E. Hueso, P. Nordlander, R. Hillenbrand, *Nano Lett.* **2011**, *11*, 3922; c) A. Yurtsever, R. M. van der Veen, A. H. Zewail, *Science* **2012**, *335*, 59; d) R. Esteban, R. Vogelgesang, J. Dorfmuller, A. Dmitriev, C. Rockstuhl, C. Etrich, K. Kern, *Nano Lett.* **2008**, *8*, 3155; e) F. De Angelis, G. Das, P. Candeloro, M. Patrini, M. Galli, A. Bek, M. Lazzarino, I. Maksymov, C. Liberale, L. C. Andreani, E. Di Fabrizio, *Nat. Nanotechnol.* **2010**, *5*, 67.
[7] a) R. L. Olmon, P. M. Krenz, A. C. Jones, G. D. Boreman, M. B. Raschke, *Opt. Express* **2008**, *16*, 20295; b) P. Alonso-Gonzalez, P. Albella, F. Golmar, L. Arzubiaga, F. Casanova, L. E. Hueso, J. Aizpurua, R. Hillenbrand, *Opt. Express* **2013**, *21*, 1270.
[8] J. D'Archangel, E. Tucker, E. Kinzel, E. A. Muller, H. A. Bechtel, M. C. Martin, M. B. Raschke, G. Boreman, *Opt. Express* **2013**, *21*, 17150.
[9] a) B. Knoll, F. Keilmann, *Opt. Commun.* **2000**, *182*, 321; b) A. Cvitkovic, N. Ocelic, R. Hillenbrand, *Opt. Express* **2007**, *15*, 8550.
[10] B. Lahiri, G. Holland, A. Centrone, *Small* **2013**, *9*, 439.
[11] a) A. Dazzi, R. Prazeres, E. Glotin, J. M. Ortega, *Opt. Lett.* **2005**, *30*, 2388; b) A. Dazzi, R. Prazeres, F. Glotin, J. M. Ortega, M. Al-Sawaftah, M. de Frutos, *Ultramicroscopy* **2008**, *108*, 635; c) J. R. Felts, K. Kjoller, M. Lo, C. B. Prater, W. P. King, *ACS Nano* **2012**, *6*, 8015.
[12] A. M. Katzenmeyer, V. Aksyuk, A. Centrone, *Anal. Chem.* **2013**, *85*, 1972.
[13] a) V. A. Fedotov, M. Rose, S. L. Prosvirnin, N. Papasimakis, N. I. Zheludev, *Phys. Rev. Lett.* **2007**, *99*, 147401; b) B. Luk'yanchuk, N. I. Zheludev, S. A. Maier, N. J. Halas, P. Nordlander, H. Giessen, C. T. Chong, *Nat. Mater.* **2010**, *9*, 707.
[14] J. R. Felts, S. Law, C. M. Roberts, V. Podolskiy, D. M. Wasserman, W. P. King, *Appl. Phys. Lett.* **2013**, *102*.
[15] C. Marcott, M. Lo, K. Kjoller, C. Prater, I. Noda, *Appl. Spectrosc.* **2011**, *65*, 1145.
[16] A. Dazzi, R. Prazeres, F. Glotin, J. M. Ortega, *Ultramicroscopy* **2007**, *107*, 1194.
[17] B. Van Eerdenbrugh, M. Lo, K. Kjoller, C. Marcott, L. S. Taylor, *Mol. Pharm.* **2012**, *9*, 1459.
[18] A. M. Katzenmeyer, J. Canivet, G. Holland, D. Farrusseng, A. Centrone, *Angew. Chem. Int. Ed.* **2014**, *53*, 2852.
[19] a) C. Mayet, A. Dazzi, R. Prazeres, E. Allot, E. Glotin, J. M. Ortega, *Opt. Lett.* **2008**, *33*, 1611; b) E. Kennedy, R. Al-Majmaie, M. Al-Rubeai, D. Zerulla, J. H. Rice, *J. Biophotonics* **2013**, DOI: 10.1002/jbio.201300138.
[20] F. Lu, M. Jin, M. A. Belkin, *Nat. Photon.* **2014**, DOI: 10.1038/nphoton.2013.373.
[21] A. Dazzi, F. Glotin, R. Carminati, *J. Appl. Phys.* **2010**, *107*, 124519.
[22] a) S. Lal, N. K. Grady, J. Kundu, C. S. Levin, J. B. Lassiter, N. J. Halas, *Chem. Soc. Rev.* **2008**, *37*, 898; b) B. Lahiri, S. G. McMeekin, R. M. De La Rue, N. P. Johnson, *Appl. Phys. Lett.* **2011**, *98*, 153116.
[23] K. Aydin, I. M. Pryce, H. A. Atwater, *Opt. Express* **2010**, *18*, 13407.
[24] B. Lahiri, A. Z. Khokhar, R. M. De La Rue, S. G. McMeekin, N. P. Johnson, *Opt. Express* **2009**, *17*, 1107.
[25] A. Dazzi, R. Prazeres, F. Glotin, J. M. Ortega, *Infrared Phys. Technol.* **2006**, *49*, 113.

© 2014 WILEY-VCH Verlag GmbH & Co. KGaA, Weinheim